ENVIRONMENTAL RESEARCH
COMMUNICATIONS

LETTER • OPEN ACCESS

Feasibility analysis of AERONET lunar AOD for nighttime particulate matter estimation

To cite this article: Kwang Nyun Kim *et al* 2023 *Environ. Res. Commun.* **5** 051004

Environmental Research Communications

LETTER

Feasibility analysis of AERONET lunar AOD for nighttime particulate matter estimation

Kwang Nyun Kim[1], **Seung Hee Kim**[2,*], **Sang Seo Park**[3] and **Yun Gon Lee**[1,*]

[1] Atmospheric Sciences, Department of Astronomy, Space Science, and Geology, Chungnam National University, Daejeon, 34134, Republic of Korea
[2] Institute for Earth, Computing, Human and Observing, Chapman University, Orange, CA 92866, United States of America
[3] Department of Urban and Environmental Engineering, Ulsan National Institute of Science and Technology (UNIST), Ulsan, 44919, Republic of Korea
[*] Authors to whom any correspondence should be addressed.

E-mail: sekim@chapman.edu **and** yglee2@cnu.ac.kr

Keywords: lunar AOD, nighttime PM estimation, AERONET AOD, random forest

OPEN ACCESS

RECEIVED
24 November 2022

REVISED
28 March 2023

ACCEPTED FOR PUBLICATION
24 April 2023

PUBLISHED
12 May 2023

Abstract

Several studies have attempted to estimate particulate matter (PM) concentrations using aerosol optical depth (AOD), based on AOD and PM relationships. Owing to the limited availability of nighttime AOD data, PM estimation studies using AOD have focused on daytime. Recently, the Aerosol Robotic Network (AERONET) produced nighttime AOD, called lunar AOD, providing an opportunity to estimate nighttime PM. Nighttime AOD measurements are particularly important as they help fill gaps in our understanding of aerosol variability and its impact on the atmosphere, as there are significant variations in AOD between day and night. In this study, the relationship between lunar AOD and PM was investigated using data from AERONET station, meteorological station, and air pollution station in Seoul Metropolitan area from May 2016 to December 2019, and then PM estimation model was developed covering both daytime and nighttime using random forest machine learning techniques. We have found the differences in the importance of variables affecting the AOD-PM relationship between day and night from the random forest model. The AOD-PM relationship in the daytime was more affected by time-related variables, such as the day of the year among the variables. The new model was developed using additional lunar AOD data to estimate continuous PM concentrations. The results have shown that the model based on lunar AOD data estimated well PM_{10} and $PM_{2.5}$ with similar performance of model using solar AOD. The results imply the possibility of seamless near-surface PM concentration data on a large scale once satellites produce nighttime AOD data.

1. Introduction

Aerosols are fine solid or liquid particles suspended in the atmosphere. They affect climate change directly (e.g., scattering Sunlight) and indirectly (e.g., condensation nuclei) (Hansen *et al* 1997, Haywood and Olivier 2000, Kaufman *et al* 2002, Change 2013, Masson-Delmotte *et al* 2021). Among aerosols, PM (particulate matter) is commonly classified into PM_{10} (10 μm or less) and $PM_{2.5}$ (2.5 μm or less) according to the optical diameter. PM_{10} and $PM_{2.5}$ are widely known to have negative effects on human health, such as premature death, respiratory disease, heart disease, and cerebrovascular disease (Suwa *et al* 2002, Gauderman *et al* 2004, Franklin *et al* 2007, Yue *et al* 2007, Zanobetti and Schwartz 2009, Apte *et al* 2015). Therefore, to prevent health and socioeconomic damage, it is necessary to understand the precise spatial and temporal variations in PM concentration, which rapidly change depending on emission, extinction, and advection over time and region.

Because the *in situ* air pollution measurement is point-based, there are spatial limitations in monitoring PM concentrations. To overcome these limitations, studies have attempted to estimate PM on the ground using

AOD retrieved from satellites with a high spatiotemporal resolution, where AOD represents the integral value of the aerosol extinction coefficient for the atmospheric optical path from the top of the atmosphere to the surface. These studies are based on the relationship between AOD and PM (PM_{10}, $PM_{2.5}$), and concentrations measured as mass concentrations of air collected from the ground. Various statistical methods, such as the linear regression model (Wang and Christopher 2003), multiple linear regression models (Liu *et al* 2005), geographically weighted regression models (Ma *et al* 2014, Bai *et al* 2016), and random forest (RF) models (Hu *et al* 2017), have been employed to improve model performance.

The relationship between AOD and PM concentrations varies spatially and temporally. AOD is the integral value of the aerosol extinction coefficient for the atmospheric optical path from the top of the atmosphere to the surface, and the PM concentration is the dry mass concentration of particles of a specific size measured at the surface. Therefore, when humidity is high, the AOD increases owing to the hygroscopic growth of the aerosol; however, the PM concentration, which is the dry mass concentration, is not affected. In addition, depending on the direction and speed of the wind on the ground, the characteristics of the aerosol particles dominating the ground surface may change or the PM concentration may change. Therefore, the relationship between AOD and PM shows a strong linear or nonlinear relationship depending on the temperature, relative humidity, wind direction, wind speed, and atmospheric boundary layer altitude.

The Aerosol Robotic Network (AERONET) is a ground-based aerosol observation network established by the National Aeronautics and Space Administration (NASA) to monitor the Earth's atmospheric aerosols (Holben *et al* 1998). AERONET uses a spectrophotometer to retrieve AOD through polarization extinction. The AERONET AOD has been used for satellite AOD data verification and calibration (Bibi *et al* 2015, Choi *et al* 2016, Bright and Christian 2019). AERONET produces daytime AOD, called solar AOD, using the Sun algorithm. In addition, it produces nighttime AOD, called lunar AOD, based on the Moon algorithm with lunar illuminance measurement (Berkoff *et al* 2011, Barreto *et al* 2013, 2016, Li *et al* 2016). The solar AOD provides final definitive level 2 data, and the lunar AOD provides level 1.5 data. Although lunar AOD provides level 1.5 data, the data quality is more reasonable than that of solar AOD based on four years of data (Perrone *et al* 2022).

Estimating PM using satellite AOD has limitations in estimating the daily averaged PM concentration because satellite AOD data are unavailable at night. However, PM has a general diurnal pattern, with peaks in the morning and at night, although there are differences from one place to another (Pérez *et al* 2010, Zhang and Cao 2015, Li *et al* 2019). Global PM2.5 concentrations exhibit homogeneous diurnal pattern. The daily cycle of PM2.5 is characterized by double peaks - a morning peak between 7:00 and 10:00 local solar time (LST), and a nighttime peak between 21:00 and 23:00 LST, and a minimum concentration in the afternoon between 15:00 and 17:00 LST (Manning *et al* 2018). Therefore, it is difficult to reflect the diurnal change in PM using AOD retrieved only during the daytime. The relationship between AOD and PM concentration varies both spatially and temporally, and PM estimation using satellite AOD has limitations in estimating average daily PM concentration because satellite AOD data is not available at nighttime.

The purpose of this study is to examine the feasibility of estimating PM at night using lunar AOD retrieved by the AERONET. The study also aims to identify variables with a strong influence on the relationship between AOD and PM concentrations, including meteorological factors and air pollutants. We examined the validity of nighttime PM estimation using lunar AOD and identify variables that affect the AOD-PM relationship between daytime and nighttime. We assessed the feasibility of PM estimation of AOD at night using lunar AOD retrieved by AERONET for the first time. In addition, by using meteorological factors and air pollutants as variables in the AOD-PM estimation model, variables with a strong influence on the AOD-PM relationship between day and night were identified. Temperature, relative humidity, wind direction, wind speed, and mixed layer height were used to consider meteorological factors, and ground observations of SO_2, NO_2, CO, and O_3 were used to evaluate the influence of the surrounding air pollutants.

Seoul is the most densely populated metropolis in the Korean Peninsula and a major city worldwide in terms of population density and industrial infrastructure. For example, Seoul has a high population density of 16,080 individuals/km^2 (https://data.seoul.go.kr/). The occurrence rate of PM in Seoul is high due to industrial and transportation factors. As a result of PM2.5, an estimated 1488 excess deaths per year occur in Seoul, and the cost of economic loss due to this death is estimated to be USD 130.79 million per year (Lee *et al* 2021). Therefore, we aimed to build a PM estimation model for Seoul.

The remainder of the sections are organized as follows: section 2 explains the data and methods used, the AOD-PM model construction method, and pre-processing; section 3 presents the results, confirms the difference in importance for each variable of the day and night time, and validates the results of the AOD-PM model and time series comparison of PM concentrations estimated by the AOD-PM model; and section 4 summarizes the results and applicability of this study.

Table 1. Site location (distance is the distance from the AERONET site to each site).

Site	Latitude (°N)	Longitude (°E)	Distance (km)
AERONET	37.56	126.93	0
KMA	37.57	126.97	2.84
AirKorea	37.58	126.94	1.39

2. Data and methods

2.1. Data

In this study, daytime and nighttime AOD-PM estimation models were developed using ground observation data of Seoul from May 2016 to December 2019. To obtain AOD data, we used the solar and lunar AOD data from the Yonsei AERONET Observatory (table 1). For solar AOD, we used level 2 500 nm AOD data retrieved from the Direct Sun Algorithm Version 3 (V3). For lunar AOD, we used level 1.5 500 nm AOD data retrieved from the Provisional Direct Moon Algorithm V3. When lunar illuminance is observed, the lunar AOD is retrieved. The AERONET V3 AOD includes fully automatic cloud screening, instrument anomaly quality controls, and a new polarized radiative transfer code, which replaces the scalar radiative transfer code of V2 (Giles *et al* 2019, Sinyuk *et al* 2020).

The Beer-Bouguer-Lambert law relates the attenuation of light to the concentration of a material through which the light passes. In the context of AOD retrieval, the law states that the amount of Sunlight or Moonlight that is absorbed or scattered by atmospheric aerosols depends on the concentration of aerosols along the path of the light (Shaw 1976, Cachorro *et al* 1987).

$$V(\lambda) = V_0(\lambda)\cdot R^{-2}\cdot e^{-\tau(\lambda)\cdot m} \tag{1}$$

The Direct Sun algorithm is based on (equation (1)) to calculate the total optical depth (τ) which is derived from measurements of the raw instrument signal at a given wavelength (V) and the signal that the photometer would have at the top of the atmosphere (V_0). The equation takes into account the Earth-Sun distance (R), the optical air mass (m) that relates to the zenith angle of the Sun, and the τ of the atmosphere. The AOD can be obtained by subtracting the contribution to extinction by all other atmospheric components, such as Rayleigh scattering and absorption by gases at the target's wavelength.

The Direct Moon algorithm uses measurements of direct lunar irradiance to retrieve AOD and is based on the lunar photometry method. Lunar photometry involves measuring the reflected solar irradiance from the Moon, which changes significantly with the Moon phase angle (MPA) and requires accurate knowledge of the extraterrestrial lunar irradiance. The Direct Moon algorithm uses the RIMO model (ROLO Implementation for Moon Observation; Barreto *et al* 2019), which is based on the ROLO (RObotic Lunar Observatory) model and the SPICE Toolkit (Acton 1996, Acton *et al* 2018), to compute the extraterrestrial lunar irradiance at various wavelengths for each observation. The lunar irradiance values are then corrected using a Román *et al* (2020) correction factor based on MPA and wavelength. The AOD is calculated using the Beer-Bouguer-Lambert law (Barreto *et al* 2013).

$$\tau_a(\lambda) = \frac{\ln[\kappa(\lambda)] - \ln\left[\frac{V(\lambda)}{I_0(\lambda)}\right] - \tau_g(\lambda)\cdot m_g - \tau_R(\lambda)\cdot m_R}{m_a} \tag{2}$$

Where the 'a' subscript stands for aerosol, 'R' for Rayleigh and 'g' for gases. Where the AOD (τ_a) is determined from calibration coefficient (κ) for a specific effective wavelength, the corrected extraterrestrial lunar irradiance (I_0) at the same wavelength, and the photometer signal (V) at the effective wavelength. The optical air masses (m) are calculated using the Kasten formula (Kasten and Young 1989) and the Moon zenith angle (MZA) as input. More details about the methodology of AOD calculation can be found in González *et al* (2020). Giles *et al* (2019) showed that the uncertainty of AERONET V3 AOD was a +0.02 bias and 1σ uncertainty of 0.02. AERONET produces AOD data at irregular intervals approximately every 3 min; thus, AOD data were converted to hourly mean data. Ge *et al* (2011) and Zhao *et al* (2012) emphasize that under certain conditions, i.e., high aerosol load and large solar zenith angle (SZA), the AOD can be erroneous due to the forward scattering effect of aerosols. To test the impact of the zenith angle, we divided the data into five categories based on the zenith angle (less than 65°, 65°–70°, 70°–75°, 75°–80°, and 80°–85°) and calculated the correlation coefficient (R value) between AOD and PM for each category. We found that the correlation coefficient varied between 0.03 to 0.1 (figure 1), suggesting that the zenith angle had a small effect on the AOD-PM relationship. While the zenith angle can have a small impact on the AOD-PM relationship, it is not a significant source of discrepancy. The total number of matched data is 5289 for solar AOD-PM_{10}, 1785 for lunar AOD-PM_{10}, 5212 for solar AOD-$PM_{2.5}$, and 1765 for

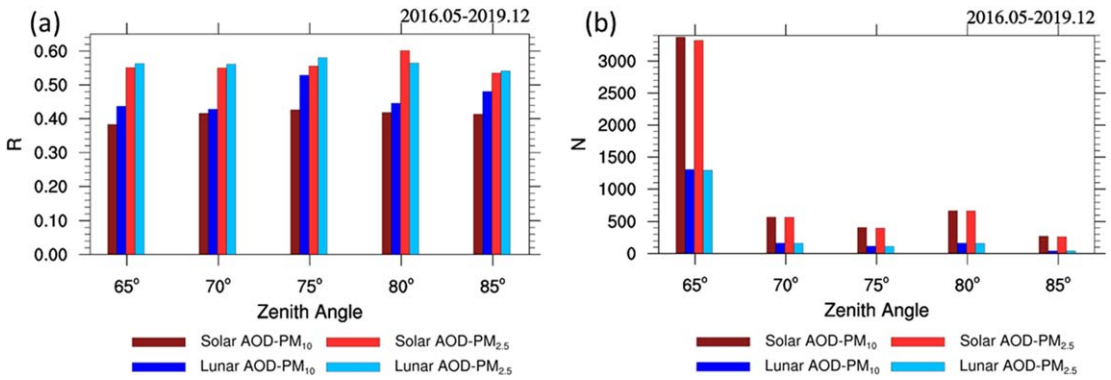

Figure 1. AOD-PM relationship according to Zenith angle (ZA) classification. ZA is divided into five categories: below 65°, 65°—70°, 70°—75°, 75°—80°, and 80°—85°. Correlation coefficient R(a) and number of data N(b) of AOD-PM are shown by category.

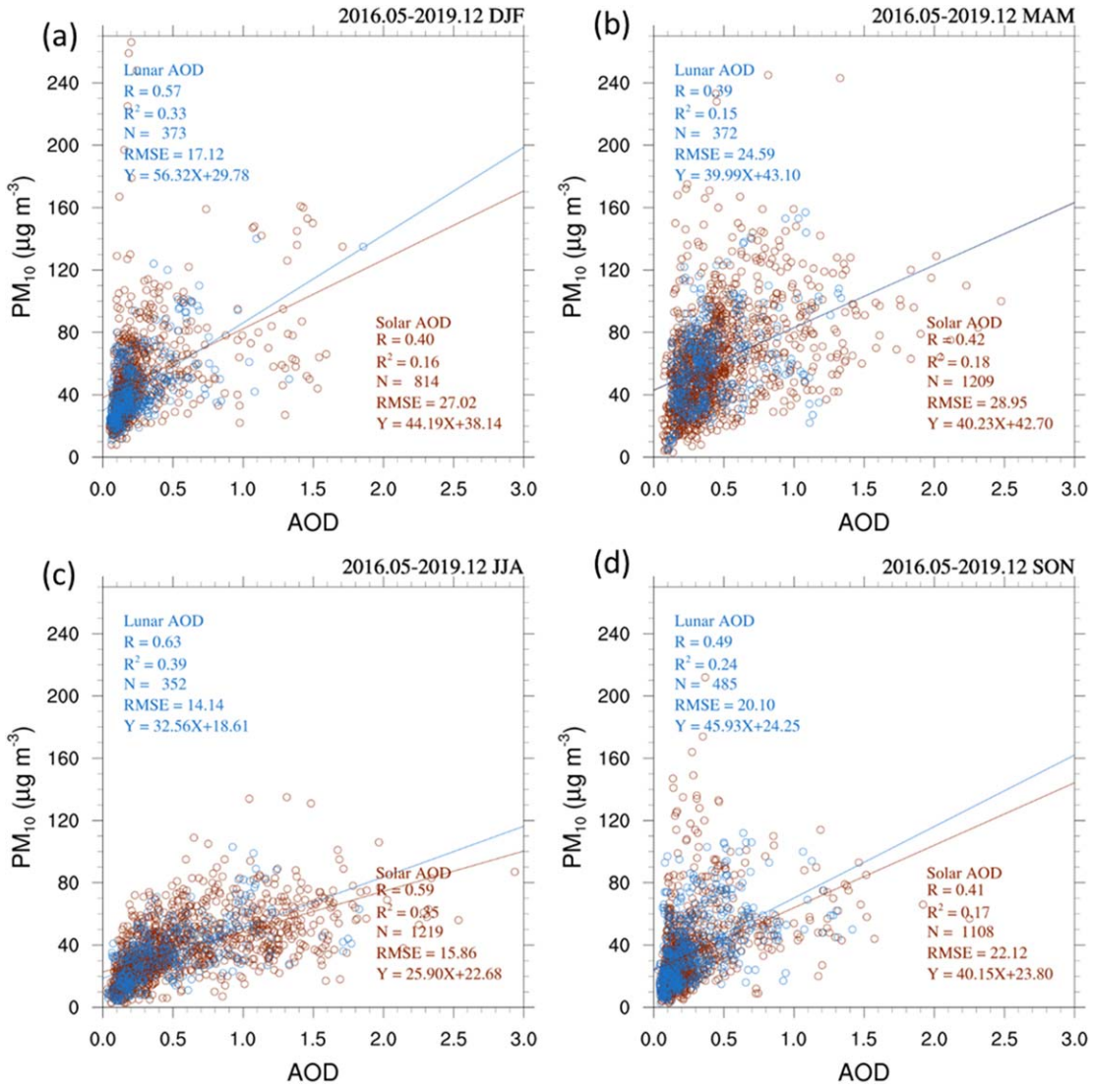

Figure 2. Relationship between seasonal solar AOD (red circle), lunar AOD (blue circle) and PM_{10} (winter (DJF)(a), spring (MAM)(b), summer (JJA)(c), and autumn (SON)(d)).

lunar AOD-$PM_{2.5}$. Compared to data matched with solar AOD, the matched data with lunar AOD is about 33%. In this study, to ensure data accuracy and avoid retrieval errors, only AOD data with solar and lunar zenith angles less than 75° were used.

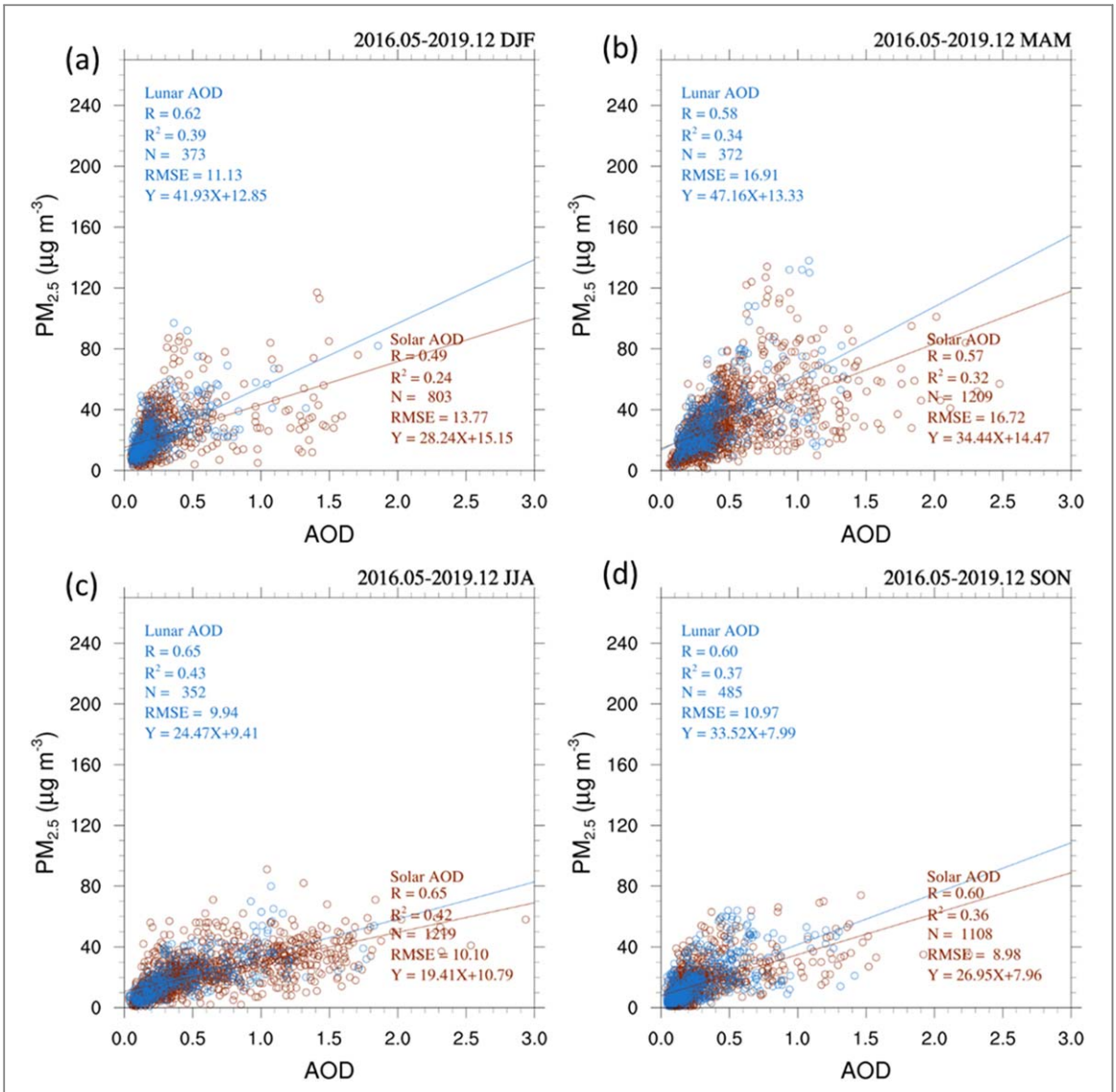

Figure 3. Relationship between seasonal solar AOD (red circle), lunar AOD (blue circle) and $PM_{2.5}$ (winter (DJF)(a), spring (MAM) (b), summer (JJA)(c), and autumn (SON)(d)).

Hourly *in situ* air pollutant data were obtained from the AirKorea website (https://www.airkorea.or.kr/). AirKorea is operated by the National Institute of Environmental Research in South Korea. Air pollution data from the AirKorea network comprised PM_{10} ($\mu g/m^3$), $PM_{2.5}$ ($\mu g/m^3$), SO_2 (ppm), NO_2 (ppm), CO (ppm), and O_3 (ppm). SO_2, NO_2, CO, and O_3 data were used as input variables for the AOD-PM model, and the effects of air pollutants on the model were examined during the day and nighttime. PM_{10} and $PM_{2.5}$ were used as dependent variables when developing each AOD-PM estimation model. The hourly air pollutant data from the AirKorea network were matched with the hourly averaged AOD values when the AERONET data were available. AirKorea was selected as the closest AERONET site (table 1).

In this study, meteorological observation data were used as input variables for the AOD-PM model to investigate the differences between AOD and day and night weather factors affecting the AOD-PM model. As meteorological observation data, hourly observation data for temperature (T), relative humidity (RH), wind direction (WD), and wind speed (WS) were obtained from the Korea Meteorological Administration's (KMA) Automated Synoptic Observing System. Mixing layer height (MLH) data retrieved using a ceilometer at Yonsei University were used as the atmospheric boundary layer altitude data. The ceilometer we used had a maximum detection height of 7.5 km and spatial resolution of 10 m and 16 s, respectively, and the MLH was retrieved from the observed aerosol backscatter vertical profile by using the gradient method (Lee *et al* 2019). The AirKorea and KMA sites used for the analysis were 1.39 km and 2.84 km away from the AERONET site, respectively, and the ceilometer for observing MLH and the AERONET site was located at Yonsei University (table 1). Meteorological and air pollutants data were recorded every hour. Each data point was matched with AERONET AOD for each hour. In addition, seasonal characteristics and daily fluctuations were considered using the day of the year

Table 2. Statistics for the solar and lunar AOD and PM_{10} relationship.

	Solar AOD						Lunar AOD					
		Mean (SD)						Mean (SD)				
	N	PM_{10}	solar AOD	Slope	Intercept	R	N	PM_{10}	lunar AOD	Slope	Intercept	R
Total	4350	45.47 (28.76)	0.4 (0.37)	30.83	33.12	0.39	1582	43.23 (24.42)	0.34 (0.28)	38.40	29.99	0.44
Winter (DJF)	814	49.93 (29.51)	0.27 (0.27)	44.19	38.14	0.4	373	43.39 (20.83)	0.24 (0.21)	56.32	29.78	0.57
Spring (MAM)	1209	61.16 (31.88)	0.46 (0.33)	40.23	42.7	0.42	372	59.42 (26.63)	0.41 (0.26)	39.99	43.1	0.39
Summar (JJA)	1219	37.28 (19.65)	0.56 (0.45)	25.9	22.68	0.59	352	33.58 (18.11)	0.46 (0.35)	32.56	18.61	0.63
Autumn (SON)	1108	34.07 (24.25)	0.26 (0.25)	40.15	23.8	0.41	485	37.69 (23.08)	0.29 (0.25)	45.93	24.25	0.49

Table 3. Statistics for the solar and lunar AOD and $PM_{2.5}$ relationship.

	Solar AOD						Lunar AOD					
		Mean (SD)						Mean (SD)				
	N	$PM_{2.5}$	solar AOD	Slope	Intercept	R	N	$PM_{2.5}$	lunar AOD	Slope	Intercept	R
Total	4287	22.59 (16.58)	0.4 (0.37)	24.94	12.53	0.55	1565	23.19 (16.65)	0.35 (0.28)	33.25	11.71	0.56
Winter (DJF)	803	22.73 (15.75)	0.27 (0.27)	28.24	15.15	0.49	373	23.04 (14.21)	0.24 (0.21)	41.93	12.85	0.62
Spring (MAM)	1209	30.33 (20.31)	0.46 (0.33)	34.44	14.47	0.57	372	32.62 (20.81)	0.41 (0.26)	47.16	13.33	0.58
Summar (JJA)	1219	21.73 (13.4)	0.56 (0.45)	19.41	10.79	0.65	352	20.59 (13.1)	0.46 (0.35)	24.47	9.41	0.65
Autumn (SON)	1108	14.91 (11.21)	0.26 (0.25)	26.95	7.96	0.6	485	17.91 (13.84)	0.29 (0.25)	33.52	7.99	0.6

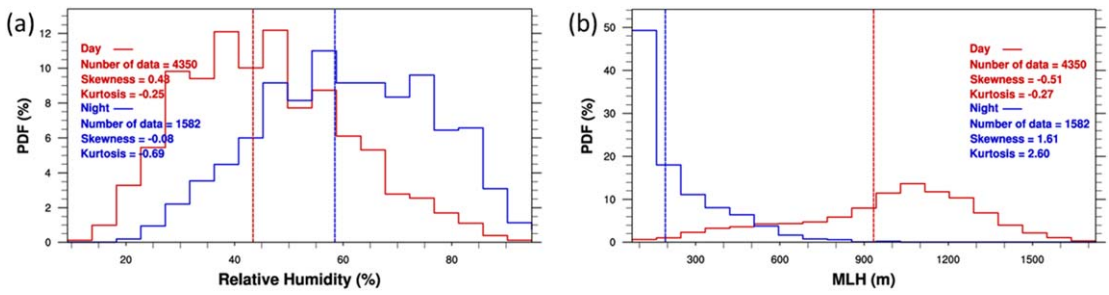

Figure 4. Day and night PDF differences of relative humidity (a) and MLH (b). The red line represents daytime data distribution, the blue line represents nighttime data distribution, and the dotted line represents the mean.

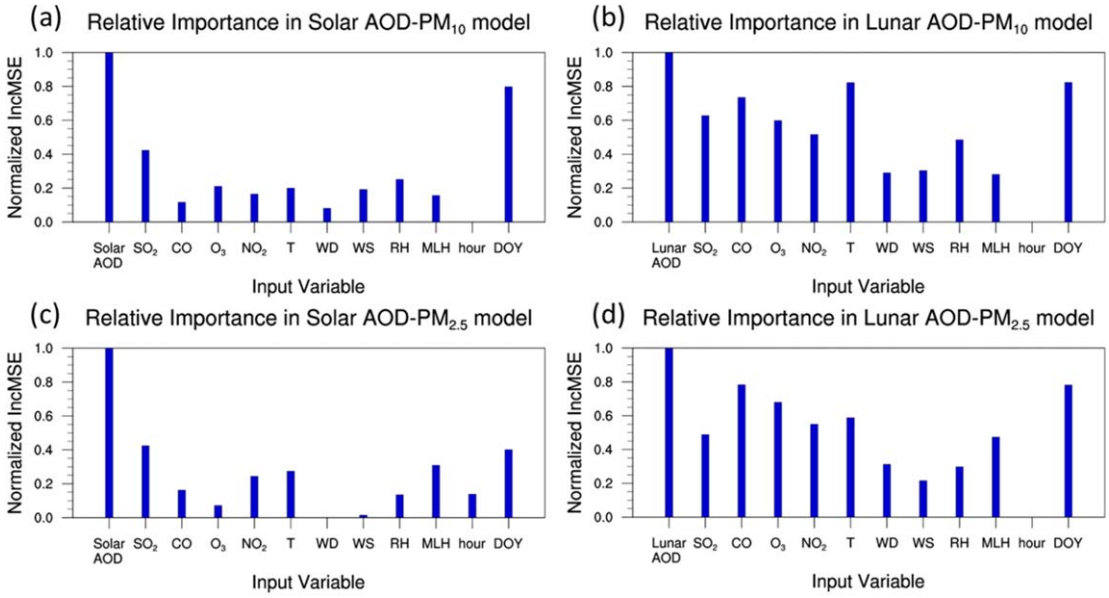

Figure 5. Variable importance for PM_{10} (a, b) and $PM_{2.5}$ (c, d) AMPT models with solar AOD and lunar AOD.

(DOY) and observation time (hours) as input variables with the time properties of the AOD-PM estimation model.

2.2. Model description

For the AOD-PM concentration estimation model, an optimal model was developed using RF, which is one of the most frequently used machine-learning techniques. RF is a classification technique that uses a meta-learning-type decision tree to extend it to multiple trees (Breiman 2001). It is an extension of the decision tree algorithm and consists of multiple decision trees to enhance the accuracy and robustness of the model. Each decision tree comprising the RF consists of randomly selected training data and input variables. In this case, the precision of the individual decision trees may be lowered, but the accuracy and stability of the RF for performing prediction by synthesizing them increases. RF has several advantages: first, the ensemble learning technique used in RF helps to increase the accuracy of the model. Second, using multiple decision trees in RF makes the data more robust against outliers and noise. Third, RF can handle high-dimensional data with many input variables. Lastly, the RF algorithm provides a measure of the importance of each input variable that can be used for feature selection. Therefore, in this study, RF was used to increase the accuracy of the AOD-PM model and to evaluate the importance of various variables during the day and night.

Meteorological factors and air pollutants influence the relationship between AOD and PM and its relative importance changes at the timing of the day. First, the differences between the day and night of the input variables were checked using a principal component analysis. The RF technique was used to calculate the importance of variables used in the model. To estimate the PM concentration through the variable importance calculated after model construction using solar AOD and lunar AOD, we checked for differences in the importance of weather factors, air pollutants, and AOD for each model.

The purpose of this study was to determine whether there was a difference in the estimated performance of the day and night AOD-PM models according to AOD, meteorological factors, air pollutants, and time variables using the constructed model. Therefore, we used the following five models: a model using only time variables (i.e., T model), a model using meteorological factors and time variables (i.e., MT model), a model using AOD and time variables (i.e., AT model), a model using air pollutants and time variables (i.e., PT model), and a model using AOD, meteorological factors, air pollutants, and time variables (i.e., AMPT model). In addition, the applicability of nighttime AOD was investigated in the estimation of PM concentration using solar AOD and lunar AOD at the Yonsei University site for approximately 3.5 years, from May 2016 to December 2019.

3. Results

3.1. AOD and PM concentration relationships

We first examined AOD-PM relationship using correlation analysis such as linear regression equation, R value, determination coefficient (R^2), and root mean square error (RMSE). In the comparison of the R value between lunar AOD-PM and solar AOD-PM relationship shows slightly higher in lunar AOD-PM_{10} and similar R value in AOD-$PM_{2.5}$. The solar AOD-PM_{10} indicate an overall good correlation between them (R = 0.39). And the lunar AOD-PM_{10} shows a better relationship than that (R = 0.44) (table 2). In the relationship between AOD and $PM_{2.5}$, both lunar AOD and solar AOD shows good correlation of R value 0.56 and 0.55, respectively (table 3).

During the study period, the averaged PM_{10} value used for solar AOD analysis was 45.47 $\mu g\,m^{-3}$ with a standard deviation (SD) of 28.76 $\mu g\,m^{-3}$, and the average value of PM_{10} matched with lunar AOD was 43.23 $\mu g\,m^{-3}$ with a SD of 24.42 $\mu g\,m^{-3}$ (table 2). The difference in concentration of PM_{10} between day and night is not large, and the concentration of $PM_{2.5}$ is similar. However, as for AOD, solar AOD appears to be ~0.06 higher than lunar AOD. While the relationship between AOD and PM varies across seasons, the patterns of both solar and lunar AOD exhibit similarities across different seasons (figures 2 and 3). These findings are in agreement with Perrone *et al* (2022), which reported similar seasonal changes between solar and lunar AOD without significant differences. Our analysis revealed a consistent pattern of the lowest slope in the seasonal AOD-PM regression equation during the summer season for both solar and lunar AOD, as presented in tables 2 and 3. This finding aligns with the study by Xie *et al* (2015), which investigated the seasonal relationship between satellite-derived AOD and PM2.5. The authors reported a lower slope during the warm season compared to the cold season, which was attributed to the lower Planetary Boundary Layer and relative humidity during the cold season.

The largest PM_{10} and $PM_{2.5}$ concentration appears in spring, but the maximum values of AOD presents in summer (tables 2, 3, figures 2, 3). The increase in PM concentration in spring is presumed to be due to the influence of fugitive dust including Asian dust events (Choi *et al* 2014), and the relatively low concentration in summer is due to frequent precipitation scavenging and less advection of polluted air masses from the west (Ghim *et al* 2001, Ghim *et al* 2015). The seasonal trend of AODs differs from that of PMs, tending to increase in the summer. Unlike PM, determined by the dry mass of particles, AODs are significantly affected by liquid water contents of the airborne particles through the scattering and absorption of light. Consequently, the high humidity levels during summer lead to higher AOD values (Yang *et al* 2019).

Although AOD and PM exhibit seasonal characteristics due to the local source and sink, the relationship between the two parameters appears consistent for both solar and lunar AOD. The finding underscores the importance of incorporating a time variable that captures seasonal variations to improve the AOD-PM estimation model performance. We have incorporated the DOY as an independent variable in the model to account for seasonal patterns and variations.

3.2. Importance of daytime and nighttime variables

Suspended aerosol particles in the atmosphere interact with meteorological parameters, consequently affecting the AOD-PM relationship. Most meteorological parameters have a strong diurnal variation thus it needs to be analyzed for the characteristics before developing PM estimation model using lunar and solar AOD that represents night and daytime respectively. Among the many meteorological variables, Temperature, RH and MLH, exhibited statistically significant disparities. Figure 4 shows the PDF differences between day and night RH and the MLH (temperature is not shown since it has same pattern as RH). Both RH and MLH showed significant differences in the day and night distributions. However, AOD and PM showed no significant differences in daytime and nighttime distributions. During the daytime, the distribution of RH was concentrated on the low side (skewness >0), and at night, the distribution was concentrated on the high side (skewness <0). The daytime average was 43.39% and the nightly average was 58.47%. The MLH has a high elevation distribution during the daytime (skewness <0) and an even distribution at various elevations at night

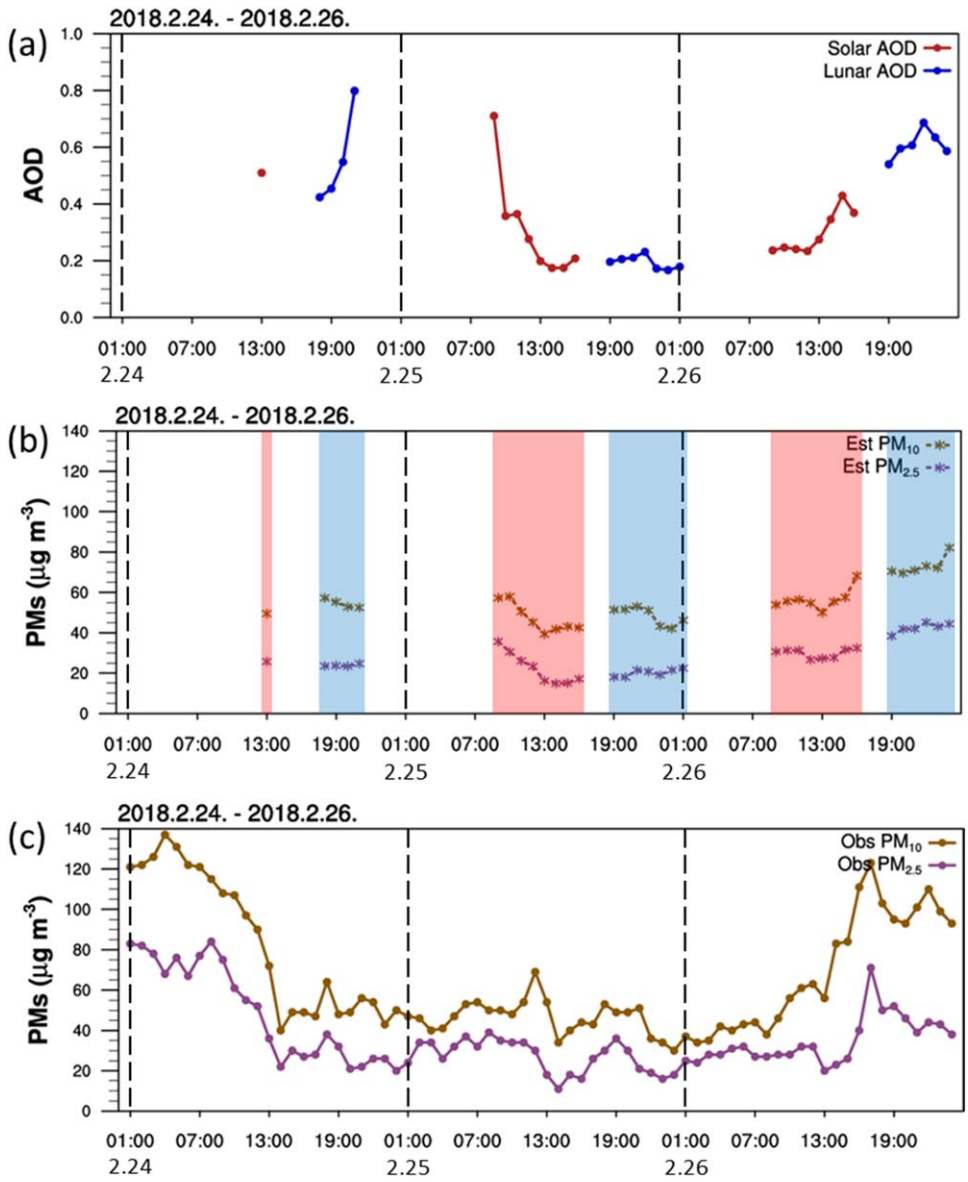

Figure 6. From February 24–26, 2018, (a) solar AOD and lunar AOD change, (b)PM concentration change estimated using solar AOD and lunar AOD, and (c) changes in PM concentration were observed. Red boxes represent times with observations from solar AOD, and the blue boxes represent times with observations from lunar AOD.

(kurtosis <0); however, at night, it had a low-altitude skewed distribution (skewness > 0) and clustered peaks at the mean value (kurtosis > 0). MLH averages 934.04 m during the day and 192.08 m at night. Differences in the distribution of these variables may affect the relationship between day and night AOD-PM. Low RH during the day limits the hygroscopic growth of aerosols, leading to a linear relationship between AOD-PM and nighttime. A low MLH at night may improve the positive correlation of AOD-PM by allowing aerosol particles to concentrate at the surface. The diurnal variation of $PM_{2.5}$ concentrations is influenced by the depth of the mixed layer and the stability of the nocturnal boundary layer. In the afternoon, the deep mixed layer leads to dilution and results in lower $PM_{2.5}$ concentrations. However, a shallow and stable nocturnal boundary layer forms after Sunset, hindering vertical mixing and allowing $PM_{2.5}$ to accumulate near the surface, leading to higher concentrations at night (Manning *et al* 2018).

The importance of the variables, according to the AMPT model, is shown in figure 5. AOD had the highest importance in all models, indicating that solar and lunar AOD are important variables when composing the AOD-PM model. During the study period, the correlation coefficient between solar AOD and PM_{10} was 0.39, and the correlation coefficient with $PM_{2.5}$ was 0.55. The correlation coefficient between lunar AOD and PM_{10} was 0.44, and that with $PM_{2.5}$ was 0.56. The correlation coefficient between the lunar AOD and PM was higher than that of the solar AOD. However, the importance of AOD was relatively higher in the daytime than in the nighttime model because the other variables did not play a notable role. The next most important variable was

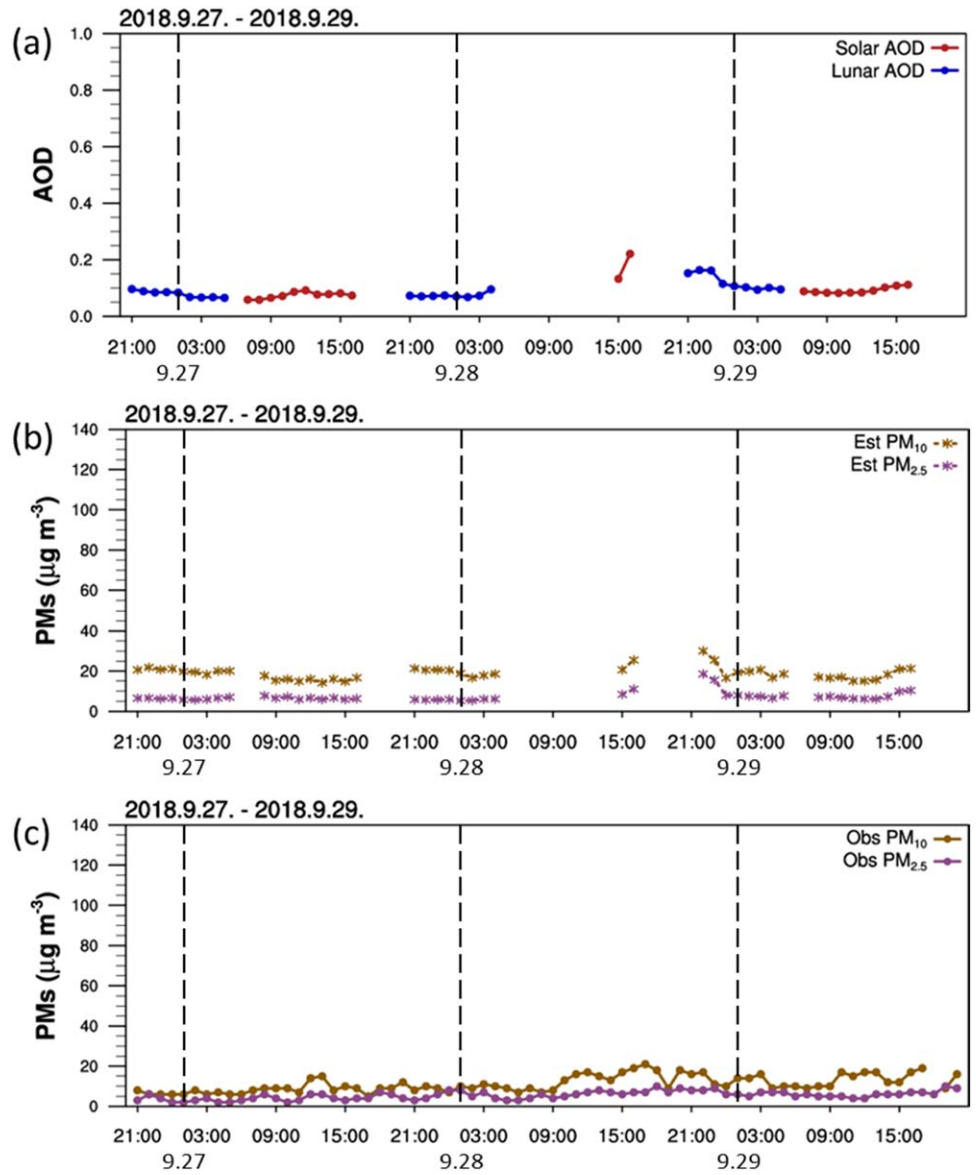

Figure 7. From September 27–29, 2018, (a) solar AOD and lunar AOD change, (b)PM concentration change estimated using solar AOD and lunar AOD, and (c) changes in PM concentration were observed.

DOY, which showed high variable importance in most of the models. Because AOD and PM exhibit seasonal fluctuations in the Korean Peninsula, it is important to apply seasonal changes to the model.

The difference between the nighttime and daytime models is that the importance of the time variable is relatively low for the nighttime model because it has a more stable atmosphere than the daytime model. Next, the importance of the variables, excluding AOD and DOY, was low in the daytime model, but there was a difference in the nighttime model. In the PM_{10} nighttime model, temperature was the second most important factor, followed by DOY, and relative humidity and air pollutants were more important in the nighttime than in the daytime. In the $PM_{2.5}$ nighttime model, CO had the highest variable importance after AOD, and variable importance was in the order of DOY, O_3, temperature, and NO_2. In the PM_{10} model, the importance of variables other than AOD was higher at night than during day. Therefore, in the nighttime model, the model estimation performance was improved by understanding the influence of each variable other than AOD in the daytime model.

3.3. Case study: PM concentration estimation

To assess the performance of the estimated PM, we have selected three distinctive cases having data both day and nighttime over 72 h. The first case was on February 24 to 26, 2018, characterized by increased PM levels during the transition from daytime to nighttime (figure 6). Figure 6(a) shows the time series of AOD, and figure 6(b) shows the time series of the PM estimates estimated using the AMPT models of solar AOD and lunar AOD.

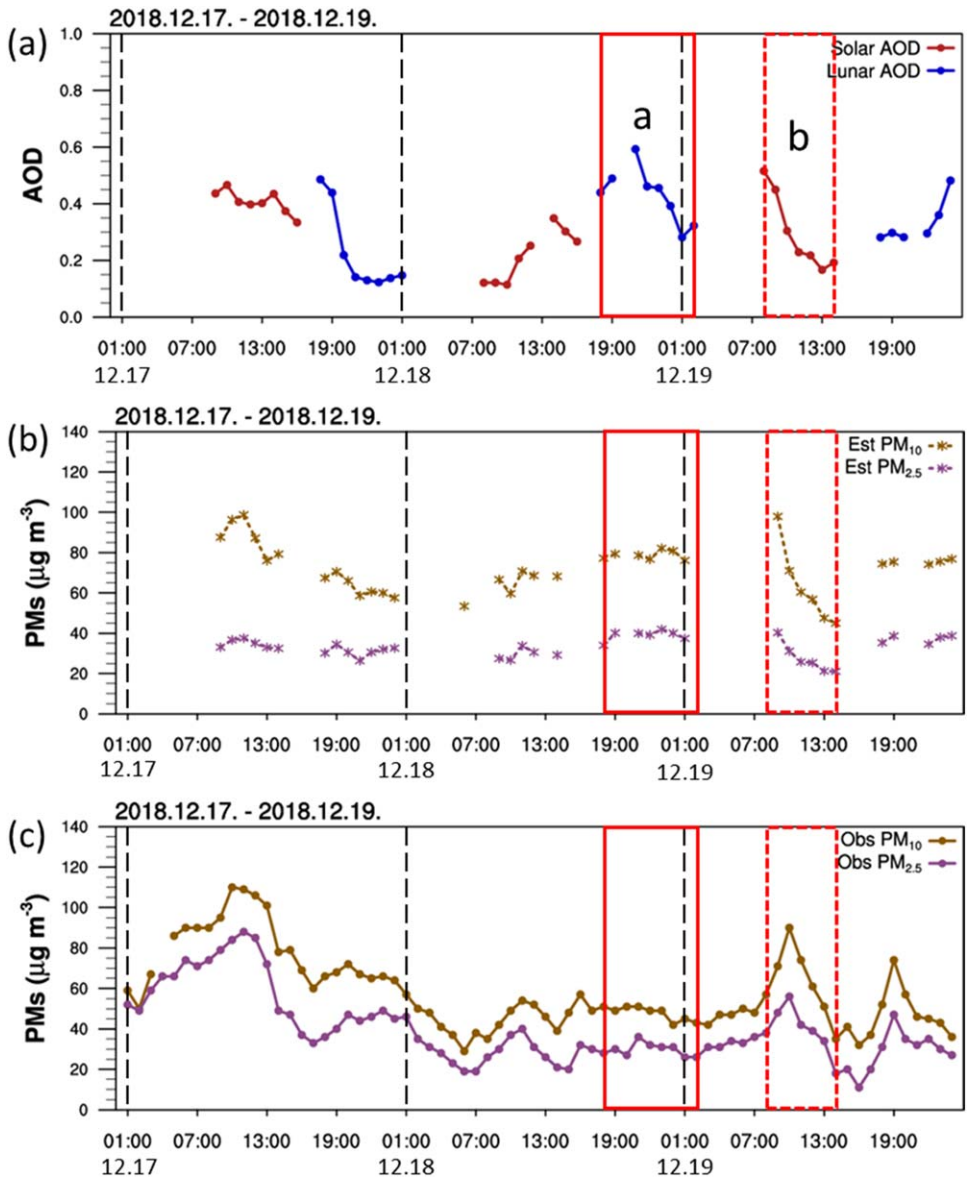

Figure 8. From December 17–19, 2018, (a) solar AOD and lunar AOD change, (b)PM concentration change estimated using solar AOD and lunar AOD, and (c) changes in PM concentration were observed. The red line box is the period when the lunar aod had a rapid change, and the red dotted line box is the period when the solar aod had a rapid change.

Figure 6(c) shows the time series of PM observations. On February 24, there was one solar AOD observation at 13:00. If only the solar AOD was used, as shown in figure 6(c) red boxes, only one estimate was calculated. PM concentration estimation can be supplemented when lunar AOD is used. Also in figure 6(b), the change in estimated value shows a decreasing trend on February 25 and an increasing trend on February 26. The observed values in figure 6(c) show the same trend as the estimated values over the same period. Thus, the estimated value correlates with the change in the observed values during day and night. The R, R^2, and RMSE of the observed and estimated PM_{10} values during the case period were 0.69, 0.83, and 5.81 $\mu g\ m^{-3}$, respectively, and those of the $PM_{2.5}$ observed and estimated values were 0.77, 0.59, and 5.7 $\mu g\ m^{-3}$, respectively. At 21:00 on February 24 and 9:00 on February 25, AOD values were higher than those before and after that time (figure 6(a)). However, regarding the observed change in PM concentration, unlike AOD, no abrupt change in the concentration was observed (figure 6(c)). In the estimated value, similar to the observed value, the change in PM concentration did not increase or decrease (figure 6(b)). The AOD and observed changes in the PM concentration did not match at 21:00 on February 24 and 9:00 on February 25. However, because the estimated PM concentration was estimated by introducing AOD rather than meteorological factors, air pollutants, and time, it might show a change similar to the observed value.

The second one is a low PM concentration case on September 27–29, 2018 (figure 7). This is under calm and stable autumn weather conditions, characterized by consistent wind speeds below 2 m s^{-1} for 72 h. During the

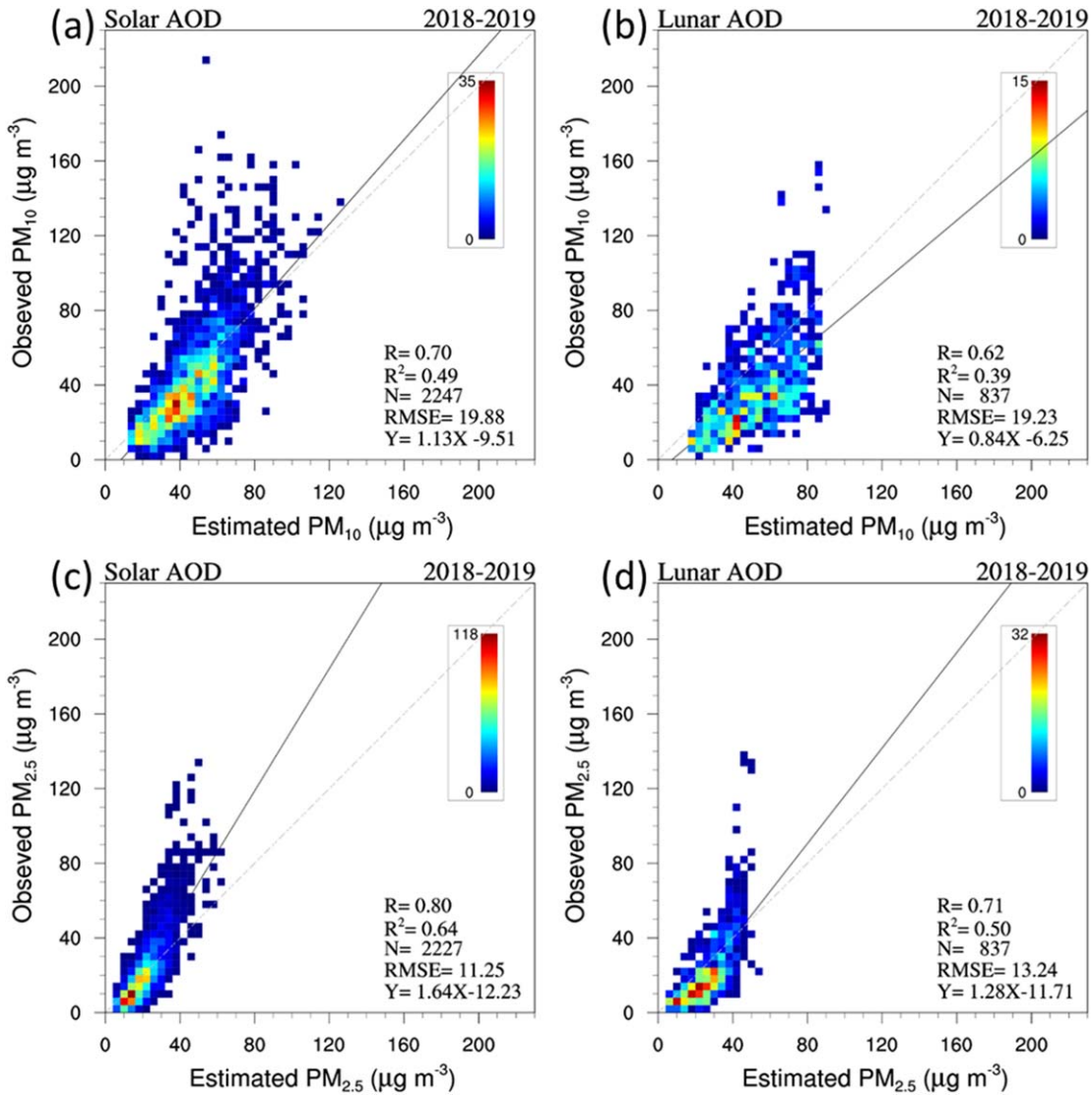

Figure 9. PM_{10}(a, b) and $PM_{2.5}$(c, d) validation results of AMPT models using solar AOD and lunar AOD. A color from blue to red indicates that the data are concentrated in that area. The solid black line represents the regression line, and the dashed gray line represents the 1:1 line.

Table 4. PM_{10} validation results for each model of solar and lunar AOD.

AOD	Solar AOD					Lunar AOD				
Model	T	MT	AT	PT	AMPT	T	MT	AT	PT	AMPT
R	0.35	0.54	0.58	0.58	0.7	0.28	0.41	0.58	0.52	0.62
R^2	0.12	0.29	0.34	0.33	0.49	0.08	0.16	0.33	0.27	0.39
RMSE	26.14	23.5	22.63	22.71	19.88	23.56	22.41	19.99	20.93	19.23
Slope	0.58	1.02	0.89	0.93	1.13	0.46	0.71	0.87	0.69	0.84
Intercept	15.7	−5.15	2.77	−3.7	−9.51	15.68	1.1	−2.63	0.66	−6.25

three-day period, both PM10 (5–21 $\mu g\,m^{-3}$) and PM2.5 (2–10 $\mu g\,m^{-3}$) maintained low concentrations. The estimated PMs showed consistently low concentrations for both PM10 and PM2.5. This case confirms that the estimated PM concentration also follows the trend well during periods of low PM concentration.

The last case presents a rapid change of AODs within 72 h. On December 17–19, 2018, substantial fluctuations were observed in both solar and lunar AOD from 0.17 to 0.52 and from 0.28 to 0.52, respectively, within a relatively short period (~8 h). The rapid alteration period in solar AOD is identified by a box delineated with a red dotted line, while lunar AOD is identified by a solid red box (figure 8). The analysis revealed that the estimated PM concentration trends were consistent with the observed PM values (figures 8(b) and (c)).

Table 5. $PM_{2.5}$ validation results for each model of solar and lunar AOD.

AOD	Solar AOD					Lunar AOD				
Model	T	MT	AT	PT	AMPT	T	MT	AT	PT	AMPT
R	0.34	0.58	0.68	0.67	0.8	0.1	0.42	0.65	0.52	0.71
R^2	0.12	0.34	0.46	0.44	0.64	0.01	0.17	0.42	0.28	0.5
RMSE	17.58	15.25	13.71	13.95	11.25	18.63	17.02	14.2	15.93	13.24
Slope	0.95	1.65	1.39	1.41	1.64	0.29	1.26	1.31	0.92	1.28
Intercept	1.32	−14.66	−6.39	−9.72	−12.23	14.69	−9.63	−9.46	−5.62	−11.71

Furthermore, during a period of rapid change in lunar AOD but observed PM has a constant value (red solid line box in figure 8), the estimated PM concentration is close to the observed PM value. The results imply that factors besides AOD can influence the estimation of PM concentrations and suggest that the accuracy of PM estimation models can be improved by considering additional variables. When the solar AOD rapidly decreased, the estimated PM decreased as well. This trend was similar to the observed PM concentrations (red dashed line box in figure 8). The results indicate that the models developed in the study well-estimate the actual PM concentrations.

In the case in which PM concentration changes during the day and at night, detecting the increase or decrease in PM concentration only by estimating the PM concentration during the daytime is difficult. In this case study, PM concentration estimation using lunar AOD helped overcome the limitations of daytime PM concentration estimation.

We identified significant differences in meteorological factors, air pollutants, and time variables that influenced the day and night AOD-PM relationships. PM concentration estimation through lunar AOD can overcome the temporal constraints of the existing AOD-PM estimation model, and the resulting data will be useful as basic data for the AOD-PM nocturnal estimation model and will help explain the spatiotemporal distribution of nighttime PM.

3.4. Validation of daytime and nighttime AOD-PM estimation model

The comparison of AMPT model results and observed PM value shows that both model constructed using solar AOD (figures 9(a) and (c)) and lunar AOD (figures 9(b) and (d)) performed well, although solar AOD-PM model has slightly higher R value than lunar AOD-PM model. For each PM, the R values of the PM_{10} estimation model (figures 9(a) and (b)) were 0.7 and 0.62 for solar and lunar AOD, respectively. $PM_{2.5}$ estimation models (figures 9(c), (d)) showed a better performance with R values of 0.8 and 0.71 for solar and lunar AOD, respectively.

Tables 4 and 5 show the verification results of the AOD-PM_{10} and AOD-$PM_{2.5}$ model by variable configuration - the T model used time variables, the MT model used time variables and meteorological factors, the AT model used time variables and AOD, the PT model used air pollutants and time variables, and the AMPT model used all variables. Regardless type of AOD and PM, AT model performs better than of T, MT, and PT model. This implies that solar and lunar AOD have a significant effect on the PM estimation model than parameters of meteorology and air pollution.

In addition, the time variable-only model (T in tables 4 and 5) shows that daytime models have a higher R value than nighttime models. The results indicate the daytime model was more affected by the time variable than the nighttime model because the PM concentration does not change significantly at night. The best model performance was by the AMPT model, implying that all meteorological factors, air pollutants, AOD, and time variables are required for optimal model performance.

4. Discussion and conclusions

In this study, the applicability of lunar AOD in estimating PM concentrations was investigated. The correlation between AOD and PM concentration varied depending on the season, with the maximum PM values are in spring but AODs in summer. The different seasonal patterns and consequent correlation between AOD and PM concentration highlight the importance of considering seasonal variations in the AOD-PM estimation model. In the model DOY was employed to reflect the seasonal component. Despite the different seasonal patterns of AOD and PM concentration, the relationship between the two parameters remained consistent for both solar and lunar AOD, highlighting the importance of considering seasonal variations in the AOD-PM estimation model. RH and MLH has strong diurnal cycle and affecting AOD-PM relationship. During the day, PDFs of RH was skewed towards lower values but skewed higher at night. The MLH had a high elevation distribution during the

day but located at lower altitudes at night, averaged MLH was 934.04 m and 192.08 respectively. Another time-related parameter—observed hour—was included in the model training to reflect diurnal patterns.

The study also revealed that solar and lunar AOD significantly influenced the estimation performance of the model, and factors besides the AODs, such as time, air pollutants, and meteorological parameters, can influence PM concentrations and consequently improve the accuracy of the estimation model. The model sensitivity tests have shown that the time variables affected solar AOD models more. Still, lunar AOD models were more affected by meteorological factors and air pollutants than solar AOD models.

Model verification results suggested that both solar AOD-PM and lunar AOD-PM models estimated PM concentrations well. When the PM concentration substantially changes in a day, the solar AOD-PM model itself cannot estimate the rapidly changing PM trend. The verification cases have revealed that the lunar AOD-MP model can provide crucial information on the prompt PM variation during nighttime.

In this study, an RF model was used to determine the importance of input variables. Regarding the variable importance, AOD was the highest, but other variables were confirmed to correct the difference between AOD and PM. RF has the advantage of extracting key variables that affect PM estimation. However, although determining the extent to which the variables affect the PM estimation is possible, this is difficult to explain. Therefore, additional analysis is necessary to determine how each variable affects the PM estimation.

The novelty of this study is that it is the first to develop a model for estimating nighttime AOD-PM using lunar AOD. Studies estimating PM have used AOD retrieved during daytime (Nordio *et al* 2013, Hu *et al* 2014, Xie *et al* 2015, Ghotbi *et al* 2016, You *et al* 2016, Lv *et al* 2017, Soni *et al* 2018, Park *et al* 2020). The Moderate Resolution Imaging Spectroradiometer (MODIS) AOD of the Terra and Aqua polar-orbiting satellites retrieves the AOD once per day according to each satellite's path. The Geostationary Ocean Color Imager (GOCI) AOD, a geostationary orbit satellite, was retrieved eight times per day from 09:00 to 16:00 KST, limited to daytime. In addition, the Cloud-Aerosol Lidar with Orthogonal Polarization AOD of the CALIPSO satellite uses Lidar measurements to retrieve AOD through polarization extinction; thus, AOD can be retrieved at night. However, because of its temporal resolution of 16 d, there is a time constraint in PM estimation.

Previous studies have limitations because only daytime PMs can be estimated using AOD. However, because continuous monitoring of PMs is required even at night, research has been conducted to estimate PM at night by observing satellite nighttime lights (Li *et al* 2015, Seo *et al* 2015, Wang *et al* 2016, Li *et al* 2017, Fu *et al* 2018, Ji *et al* 2018, Ji *et al* 2019, Park *et al* 2019, Wang *et al* 2021). However, because lunar illuminance affects night illuminance, PM estimation studies using night illuminance have selected days with low lunar illuminance to avoid the influence of the Moon on constructing and evaluating a model. Therefore, PMs can only be estimated on days with low lunar illuminance.

PM estimation at night using lunar AOD can supplement the limitations of PM estimation through nighttime light and improve the understanding of daily fluctuations of PMs and changes in the relationship between day and night AOD-PM. In addition, the literature overcomes the time constraints of the AOD-PM daytime estimation model. Notably, research is underway to retrieve AOD using lunar illuminance at night (Zhou *et al* 2021), which is useful as basic data for generating a nighttime PM spatial map using the AOD-PM nighttime estimation model. Therefore, the results of this study may help to overcome the spatiotemporal limitations of PM concentration monitoring.

The current study has employed the AOD data with a zenith angle range from 0 to 75 degrees following previous studies. Future studies need to investigate the effects of a larger zenith angle value on the AOD-PM models. Another limitation of this study is that the correlation between AOD and PM concentration was investigated at a single location (Seoul). A more comprehensive study needs to be conducted in multiple locations to validate the model's accuracy and effectiveness under various environmental conditions. The model sensitivity tests have been done with limited variables, such as time, meteorological parameters, and air pollutants. Other factors, such as land use and topography, affecting the AOD-PM relationship should also be considered to enhance the accuracy of the model. Also, we have utilized a single machine learning model (RF) in this study. Many advanced machine learning techniques have been developed as the methods became popular tools in scientific analysis. In future studies, utilizing multiple machine learning models may improve the AOD-PM model performance in addition to the lunar AOD data.

Data availability statement

The data cannot be made publicly available upon publication because no suitable repository exists for hosting data in this field of study. The data that support the findings of this study are available upon reasonable request from the authors.

Acknowledgments

This research was supported by a grant from the National Institute of Environment Research (NIER), funded by the Ministry of Environment (MOE) of the Republic of Korea (grant no. NIER-2023-01-02-094).

ORCID iDs

Kwang Nyun Kim https://orcid.org/0000-0002-9931-6069
Seung Hee Kim https://orcid.org/0000-0002-5949-8996
Yun Gon Lee https://orcid.org/0000-0002-1187-6206

References

Acton C *et al* 2018 A look towards the future in the handling of space science mission geometry *Planet. Space Sci.* **150** 9–12
Acton C H Jr 1996 Ancillary data services of NASA's navigation and ancillary information facility *Planet. Space Sci.* **44** 65–70
Apte J S *et al* 2015 Addressing global mortality from ambient PM2. 5 *Environmental Science & Technology* **49** 8057–66
Bai Y *et al* 2016 A geographically and temporally weighted regression model for ground-level PM2. 5 estimation from satellite-derived 500 m resolution AOD *Remote Sensing* **8** 262
Barreto A *et al* 2013 A new method for nocturnal aerosol measurements with a lunar photometer prototype *Atmos. Meas. Tech.* **6** 585–98
Barreto A *et al* 2016 The new sun-sky-lunar cimel CE318-T multiband photometer–a comprehensive performance evaluation *Atmos. Meas. Tech.* **9** 631–54
Barreto A *et al* 2019 Evaluation of night-time aerosols measurements and lunar irradiance models in the frame of the first multi-instrument nocturnal intercomparison campaign *Atmos. Environ.* **202** 190–211
Berkoff T A *et al* 2011 Nocturnal aerosol optical depth measurements with a small-aperture automated photometer using the Moon as a light source *J. Atmos. Oceanic Technol.* **28** 1297–306
Bibi H *et al* 2015 Intercomparison of MODIS, MISR, OMI, and CALIPSO aerosol optical depth retrievals for four locations on the Indo-Gangetic plains and validation against AERONET data *Atmos. Environ.* **111** 113–26
Breiman L 2001 Random forests *Mach. Learn.* **45** 5–32
Bright J M and Christian A G 2019 Climate-specific and global validation of MODIS Aqua and Terra aerosol optical depth at 452 AERONET stations *Sol. Energy* **183** 594–605
Cachorro V E, de Frutos A M and Casanova J L 1987 Determination of the Angstrom turbidity parameters *Appl. Opt.* **26** 3069–76
Change, IPCC Climate 2013 The physical science basis *Contribution of Working Group I to the Fifth Assessment Report of the Intergovernmental Panel on Climate Change* **1535** 2013
Choi S-H *et al* 2014 Behavior of particulate matter during high concentration episodes in Seoul *Environmental Science and Pollution Research* **21** 5972–82
Choi M *et al* 2016 GOCI Yonsei Aerosol Retrieval (YAER) algorithm and validation during the DRAGON-NE Asia 2012 campaign *Atmos. Meas. Tech.* **9** 1377–98
Franklin M, Zeka A and Schwartz J 2007 Association between PM2. 5 and all-cause and specific-cause mortality in 27 US communities *J. Exposure Sci. Environ. Epidemiol.* **17** 279–87
Fu D *et al* 2018 Mapping nighttime PM2. 5 from VIIRS DNB using a linear mixed-effect model *Atmos. Environ.* **178** 214–22
Gauderman W J *et al* 2004 The effect of air pollution on lung development from 10 to 18 years of age *New Engl. J. Med.* **351** 1057–67
Ge J M *et al* 2011 Dust aerosol forward scattering effects on ground-based aerosol optical depth retrievals *J. Quant. Spectrosc. Radiat. Transf.* **112** 310–9
Ghim Y, Sung H S, Oh and Chang Y-S 2001 Meteorological effects on the evolution of high ozone episodes in the greater Seoul area *J. Air Waste Manage. Assoc.* **51** 185–202
Ghim Y, Sung Y-S, Chang and Jung K 2015 Temporal and spatial variations in fine and coarse particles in Seoul, Korea *Aerosol Air Qual. Res.* **15** 842–52
Ghotbi S, Sotoudeheian S and Arhami M 2016 Estimating urban ground-level PM10 using MODIS 3km AOD product and meteorological parameters from WRF model *Atmos. Environ.* **141** 333–46
Giles D M *et al* 2019 Advancements in the Aerosol Robotic Network (AERONET) Version 3 database–automated near-real-time quality control algorithm with improved cloud screening for Sun photometer aerosol optical depth (AOD) measurements *Atmos. Meas. Tech.* **12** 169–209
González R *et al* 2020 Daytime and nighttime aerosol optical depth implementation in CÆLIS.' Geoscientific Instrumentation *Methods and Data Systems* **9** 417–33
Hansen J, Sato M and Ruedy R 1997 Radiative forcing and climate response *Journal of Geophysical Research: Atmospheres* **102** 6831–64
Haywood J and Olivier B 2000 Estimates of the direct and indirect radiative forcing due to tropospheric aerosols: a review *Rev. Geophys.* **38** 513–43
Holben B N *et al* 1998 AERONET—A federated instrument network and data archive for aerosol characterization *Remote Sens. Environ.* **66** 1–16
Hu X *et al* 2014 Estimating ground-level PM2. 5 concentrations in the Southeastern United States using MAIAC AOD retrievals and a two-stage model *Remote Sens. Environ.* **140** 220–32
Hu X *et al* 2017 Estimating PM2. 5 concentrations in the conterminous United States using the random forest approach *Environmental Science & Technology* **51** 6936–44
Ji G *et al* 2019 Detecting spatiotemporal dynamics of PM2. 5 emission data in China using DMSP-OLS nighttime stable light data *J. Clean. Prod.* **209** 363–70
Ji G *et al* 2018 Exploring China's 21-year PM10 emissions spatiotemporal variations by DMSP-OLS nighttime stable light data *Atmos. Environ.* **191** 132–41
Kasten F and Young A T 1989 Revised optical air mass tables and approximation formula *Appl. Opt.* **28** 4735–8
Kaufman Y J, Tanré D and Boucher O 2002 A satellite view of aerosols in the climate system *Nature* **419** 215–23

Lee J *et al* 2019 Ceilometer monitoring of boundary-layer height and its application in evaluating the dilution effect on air pollution *Boundary-Layer Meteorology* **172** 435–55
Lee Y *et al* 2021 Economic damage cost of premature death due to fine particulate matter in Seoul, Korea *Environmental Science and Pollution Research* **28** 51702–13
Li Z *et al* 2016 Simple transfer calibration method for a Cimel Sun–Moon photometer: calculating lunar calibration coefficients from Sun calibration constants *Appl. Opt.* **55** 7624–30
Li R, Liu X and Li X 2015 Estimation of the PM2. 5 pollution levels in Beijing based on nighttime light data from the defense meteorological satellite program-operational linescan system *Atmosphere* **6** 607–22
Li X *et al* 2019 Particulate matter pollution in Chinese cities: areal-temporal variations and their relationships with meteorological conditions (2015–2017) *Environ. Pollut.* **246** 11–8
Li X *et al* 2017 Evaluating the use of DMSP/OLS nighttime light imagery in predicting PM2. 5 concentrations in the northeastern United States *Remote Sensing* **9** 620
Liu Y *et al* 2005 Estimating ground-level PM2. 5 in the eastern United States using satellite remote sensing *Environmental Science & Technology* **39** 3269–78
Lv B *et al* 2017 Daily estimation of ground-level PM2. 5 concentrations at 4 km resolution over Beijing-Tianjin-Hebei by fusing MODIS AOD and ground observations *Sci. Total Environ.* **580** 235–44
Ma Z *et al* 2014 Estimating ground-level PM2. 5 in China using satellite remote sensing *Environmental Science & Technology* **48** 7436–44
Manning M I *et al* 2018 Diurnal patterns in global fine particulate matter concentration *Environmental Science & Technology Letters* **5** 687–91
Masson-Delmotte V *et al* 2021 Climate change 2021: the physical science basis *Contribution of Working Group I to the Sixth Assessment Report of the Intergovernmental Panel on Climate Change* 2
Nordio F *et al* 2013 Estimating spatio-temporal resolved PM10 aerosol mass concentrations using MODIS satellite data and land use regression over Lombardy, Italy *Atmos. Environ.* **74** 227–36
Park S *et al* 2019 Estimation of ground-level particulate matter concentrations through the synergistic use of satellite observations and process-based models over South Korea *Atmos. Chem. Phys.* **19** 1097–113
Park S *et al* 2020 Estimation of spatially continuous daytime particulate matter concentrations under all sky conditions through the synergistic use of satellite-based AOD and numerical models *Sci. Total Environ.* **713** 136516
Pérez N *et al* 2010 Variability of particle number, black carbon, and PM10, PM2. 5, and PM1 levels and speciation: influence of road traffic emissions on urban air quality *Aerosol Sci. Technol.* **44** 487–99
Perrone M R, Lorusso A and Romano S 2022 Diurnal and nocturnal aerosol properties by AERONET Sun-sky-lunar photometer measurements along four years *Atmos. Res.* **265** 105889
Román R *et al* 2020 Correction of a lunar-irradiance model for aerosol optical depth retrieval and comparison with a star photometer *Atmos. Meas. Tech.* **13** 6293–310
Shaw G E 1976 Error analysis of multi-wavelength Sun photometry *Pure Appl. Geophys.* **114** 1–14
Sinyuk A *et al* 2020 The AERONET Version 3 aerosol retrieval algorithm, associated uncertainties and comparisons to Version 2 *Atmos. Meas. Tech.* **13** 3375–411
Seo S *et al* 2015 Estimation of PM 10 concentrations over Seoul using multiple empirical models with AERONET and MODIS data collected during the DRAGON-Asia campaign *Atmos. Chem. Phys.* **15** 319–34
Soni M, Payra S and Verma S 2018 Particulate matter estimation over a semi arid region Jaipur, India using satellite AOD and meteorological parameters *Atmospheric Pollution Research* **9** 949–58
Suwa T *et al* 2002 Particulate air pollution induces progression of atherosclerosis *J. Am. Coll. Cardiol.* **39** 935–42
Wang J and Christopher S A 2003 Intercomparison between satellite-derived aerosol optical thickness and PM2. 5 mass: implications for air quality studies *Geophys. Res. Lett.* **30**
Wang J *et al* 2016 Potential application of VIIRS Day/Night Band for monitoring nighttime surface PM2. 5 air quality from space *Atmos. Environ.* **124** 55–63
Wang Y *et al* 2021 Estimation and analysis of the nighttime PM2. 5 concentration based on LJ1-01 images: a case study in the pearl river delta urban agglomeration of China *Remote Sensing* **13** 3405
Xie Y *et al* 2015 Daily estimation of ground-level PM2. 5 concentrations over Beijing using 3 km resolution MODIS AOD *Environmental science & technology* **49** 12280–8
Yang Q *et al* 2019 The relationships between PM2. 5 and aerosol optical depth (AOD) in mainland China: about and behind the spatio-temporal variations *Environ. Pollut.* **248** 526–35
Yue W *et al* 2007 Ambient source-specific particles are associated with prolonged repolarization and increased levels of inflammation in male coronary artery disease patients *Mutation Research/Fundamental and Molecular Mechanisms of Mutagenesis* **621** 50–60
You W *et al* 2016 Estimating national-scale ground-level PM25 concentration in China using geographically weighted regression based on MODIS and MISR AOD *Environmental Science and Pollution Research* **23** 8327–38
Zanobetti A and Schwartz J 2009 The effect of fine and coarse particulate air pollution on mortality: a national analysis *Environ. Health Perspect.* **117** 898–903
Zhang Y-L and Cao F 2015 Fine particulate matter (PM2. 5) in China at a city level *Sci. Rep.* **5** 1–12
Zhao F *et al* 2012 The effect and correction of aerosol forward scattering on retrieval of aerosol optical depth from Sun photometer measurements *Geophys. Res. Lett.* **39** 14
Zhou M *et al* 2021 Nighttime smoke aerosol optical depth over US rural areas: first retrieval from VIIRS Moonlight observations *Remote Sens. Environ.* **267** 112717